 ICES-2023-365

Nuclear Data Needs for GCR Shielding Models

Lawrence H. Heilbronn[1]
University of Tennessee, Knoxville, Tennessee, 37902

Fundamental nuclear data, such as differential and total cross sections, are critical in the development and improvement of calculational tools used to predict the dose and risk from exposure to galactic cosmic rays (GCR). Those tools include complex Monte Carlo transport codes as well as 3-dimensional analytical codes, all of which rely on an accurate description of the nuclear interactions between the incoming GCR ion and the target nuclei it strikes. As shielding thickness increases, calculations indicate that secondary light ions such as protons, deuterons, tritons, 3-He, 4-He and neutrons become the dominant source of the radiation field behind the shielding. When comparing predictions of doses and particle fluences behind thick shielding between several different codes, differences up to 20 percent or more are observed, mostly due to the prediction of secondary light ions from GCR interactions. The range of GCR ion species and energies along with the range of shielding materials creates a potentially large set of differential and total reaction cross sections to consider when improving code predictions. The available data base of measured cross sections will be presented, along with recommendations for additional cross section measurements needed to reduce uncertainties and improve the accuracy of radiation transport models used for GCR shielding.

Nomenclature

FLUKA = FLUktuierende KAskade
GeV = Giga electron Volts (10^9 electron Volts)
GCR = Galactic Cosmic Rays
GEANT = Gigabit European Academic Network
HZE = High-Z (atomic number), high-energy nuclei in the GCR
HZETRN = HZE Transport
LEO = Low-Earth Orbit
MCNP = Monte Carlo N-Particle
MeV = Mega electron Volts (10^6 electron Volts)
NASA = National Aeronautics and Space Administration
PHITS = Particle and Heavy Ion Transport code System
SEP = Solar Energetic Particles
SPE = Solar Particle Events

I. Introduction

THE radiation environment in space is complex, consisting of galactic cosmic rays (GCR), solar energetic particles (SEP), and trapped belt radiation around planets with an appreciable magnetic field. For crewed missions beyond low-Earth orbit (LEO), both GCR and SEP present risks to crew and electronics, but in different ways. GCR ions are present at all times, although their intensities vary with solar cycle, where the GCR flux is at a maximum during solar minimum, and at decreased intensities during solar maximum. SEP, on the other hand, are generated by solar particle events (SPE), with events lasting from one day to two or more weeks, depending on the event. The GCR and SEP energy spectra are different, as well. GCR ion energies range from keV per nucleon up to several tens of TeV per nucleon, with ion species ranging primarily from protons to nickle ions[1–3]. Protons comprise approximately 89-90 percent of the GCR flux, He comprises 8-9 percent, and the remaining 1-2% are ions heavier than He, with the flux dropping sharpley after Fe and Ni ions. SEP spectra are primarly protons with energies up to a few hundred of MeV, with the majority of the flux below 100 MeV. SEP flux is higher than GCR flux, but due to the short term of those events and the

[1] John D. Tickle Professor, Nuclear Engineering Department, 421 Zeanah Engineering Complex, 863 Neyland Dr., Knoxville, TN 37902

relatively lower energies, GCR contributes more dose than SEP over an extended mission. The primary concern from SEP in terms of risk to the mission is an acute dose leading to deterministic effects if adequate shielding is not present. Because the majority of SEP flux is from relatively low-energy protons, adequate shielding can be implemented in most mission scenarios.

The radiation environment for crewed operations in space will be composed both of primary particles with enough energy to penetrate shielding and the secondary particles created by nuclear interactions between the primary ion and the atomic nuclei in the material. In addition to nuclear interactions, charged particles will slow down via coulomb interactions with atomic electrons in the material (stopping power). Stopping power interactions at these energies are generally well understood and are not the focus of this study. The nuclear interactions, on the other hand, create a complex secondary particle flux that is less understood. When considering GCR ions, these interactions will occur over a wide range of particle energies and particle species, and as such, the evaluation of risk from the radiation environment behind shielding must rely on radiation transport models, both Monte Carlo and analytical, deterministic codes, to predict the doses and subsequent risk from exposure in those shielding environments. The codes used for GCR interactions depend on physics models to describe the interactions, and those models depend on a reliable data base of cross section measurements and thick-target yields for verification and validation of model predictions. A lack of cross section and thick-target yield data on the production of secondary light ions is the greatest source of uncertainty in GCR transport calculations and is the subject of this study.

The calculated yields of secondary light ions (protons, deuterons, tritons, 3He, 4He and neutrons) have been predicted to contribute 50% of the dose equivalent behind 5 g/cm2 of Al and 80% of the dose equivalent behind 30 g/cm2 of Al [13].

II. Secondary Light-Ion Production from GCR Interactions

High energy, heavy-ion GCR ions (HZE, refers to ions with $Z \geq 2$) create secondary particles via breakup of both the incoming HZE particle and the target nucleus it strikes. The breakup of the projectile and target can create energetic heavy fragment ions (fragments heavier than helium) and secondary protons, deuterons, tritons, ^{3}He, ^{4}He and neutrons, referred to here as secondary light ions. A study by Slaba et al.[4] conducted a comparison of the predictions of dose, dose equivalent and effective dose from several transport models, including PHITS[5], MCNP6[6-7], Geant4[8], FLUKA[9], and the NASA code HZETRN[10-11]. Separate calculations were run for aluminum shielding and polyethylene shielding as a function of shielding thickness. Aluminum was chosen because of its extensive use in spacecraft design. Polyethylene was chosen for its superior performance as a GCR shielding material, although it is not a good structural material.

Figure 1 below is from Ref. 4 and shows the dose equivalent as a function of aluminum shielding thickness (left plot) and polyethylene thickness (right plot), with thickness in units of g/cm2. The critical feature of these calculations is that they were done in an enclosed environment. Thus, incoming GCR ions that strike the forward wall of the enclosed space can (1) penetrate and interact in the back wall, and (2) created secondary ions in the forward wall that also penetrate and interact in the back wall, with the interactions in the back wall creating an albedo spectrum on light ions in the enclosed space. The increase in dose equivalent in the aluminum results beyond 20-30 g/cm^2 is found to be due to the buildup of secondary light ions, with protons contributing to about 70% of the buildup. Calculations with polyethylene show similar results, although the dose equivalent remains constant beyond 20-30 g/cm^2. Both results indicate a minimum dose equivalent and optimial shielding thickness round 20-30 g/cm^2. These results also indicate that there is no utility in adding shielding between 20-30 g/cm^2 and 100 g/cm^2, suggesting an optimaization in mission cost when considering launching shielding into space.

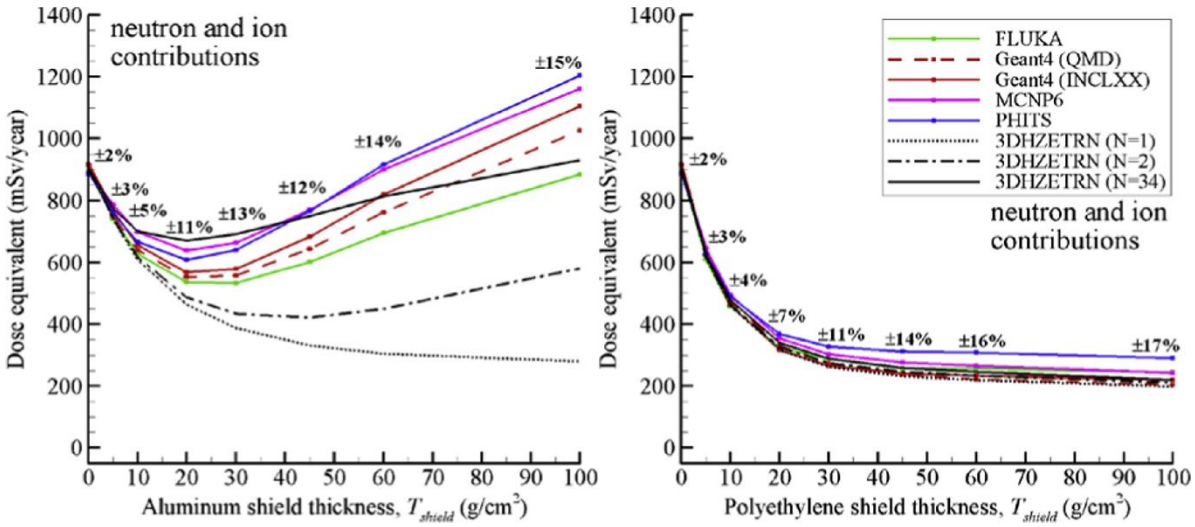

Figure 1. Dose equivalent from GCR irradiation behind the given thicknesses of aluminum shielding (left plot) and polyethylene shielding (right plot), as calculated by the indicated radiation transport models. The percentages are calculated as half the difference of the extreme model results divided by the average of the extremes.

III. Data Needs for Secondary Charged Light Ion Production

Norbury et al. have published extensive studies on existing experimental measurements of double-differential cross sections relevant to GCR interactions[12-15]. The results of those studies are summarized in Ref. 16 and are listed verbatim here:

• In the low energy region below the pion threshold (<280 MeV/n), double differential cross sections for light ion production mainly exist for H, He, C, O, Ne, and Ar projectiles.

• In the medium energy (280–3,000 MeV/n) region, double differential cross sections for light ion production mainly exist for H, He, C, Ne, and Ar projectiles.

• In the high energy (3–15 GeV/n) and very high energy (>15 GeV/n) regions, there are no double differential cross-section data for light ion production.

• Even though there are a moderate number of experimental measurement articles dealing with helium projectiles, further detailed analysis of He data below 3 GeV/n reveals significant problems and flaws with the data, leading to the conclusion that there is almost no high-quality double differential data for helium projectiles over the entire energy region.

• No double differential cross section data exist for light ion fragment production from helium projectiles above 3 GeV/n.

• No double differential cross section data exist for light ion fragment production from oxygen projectiles above the pion threshold (> 280 MeV/n).

• No double differential cross section data exist for light ion fragment production from silicon projectiles in any energy region.

Reference 16 notes that no data for secondary light ion cross sections exists for Fe projectiles, but it's noted that this refers to charged secondary light ions. Data does exist for double differential neutron spectra from Fe projectiles (see next section). Given the significance of iron in the GCR spectrum, there is an obvious need for charged secondary light ion double differential cross sections from Fe projectiles, in addition to data needs at high energies (above 3 GeV/nucleon) and He projectile data.

IV. Data Needs for Secondary Neutron Production Cross Sections and Thick-Target Yields

Measurements of secondary neutron production cross sections and thick target yields at accelerator facilities have also provided data for validation and verification of the codes' abilities to predict the neutron environment created by GCR and SEP interactions. Table I shows a list of secondary neutron cross sections produced from heavy-ion

interactions at energies relevant to GCR transport in various targets[17]. Beam energies are in units of MeV/nucleon. Targets include elemental targets, polyethylene, and the composite marsbar target composed of 85% simulated Martian regolith and 15% polyethylene. Where indicated, double-differential cross sections ("ddx"), differential angular spectra (n/dΩ) and total cross sections were measured. The fourth column indicates the laboratory angles where data was measured, and Emin indicates the lower threshold neutron energy at the corresponding angle. The accelerator facility is indicated in the last column.

Table I. Details of secondary neutron production cross sections from heavy ion interactions relevant to GCR transport. (From Ref. 17}

Beam ion and energy (MeV/nucleon)	Targets	Measured spectra	θ (deg)	Emin (MeV)	Facility
He (135)	C, Al, Cu, Pb	ddx n/dΩ total	0, 15, 30, 50, 80, 110	10 (all angles)	RIKEN
He (230)	Al, Cu	ddx n/dΩ total	5, 10, 20, 30, 40, 60, 80	5.5, 5, 4, 3.5, 3.5, 3	HIMAC (PH2)
C (135)	C, Al, Cu, Pb	ddx n/dΩ total	0, 15, 30, 50, 80, 110	10 (all angles)	RIKEN
C (290)	C, Cu, Pb, marsbar	ddx n/dΩ total	5, 10, 20, 30, 40, 60, 80	10, 3, 3, 7, 4, 3, 3	HIMAC (SB3)
C (400)	Li, C, CH_2, Al, Cu, Pb	ddx n/dΩ total	5, 10, 20, 30, 40, 60, 80	8.5, 5, 3.5, 3, 3, 3	HIMAC (PH2 and SB3)
N (400)	C, Cu	ddx n/dΩ total	5, 10, 20, 30, 40, 60, 80	6, 6, 5, 5.5, 5.5, 5	HIMAC (PH2)
Ne (135)	C, Al, Cu, Pb	ddx n/dΩ total	0, 15, 30, 50, 80, 110	10 (all angles)	RIKEN
Ne (337)	C, Al, Cu, U	ddx total	30, 45, 60, 90	12 (all angles)	LBL Bevalac
Ne (400)	C, Cu, Pb, ISS wall	ddx n/dΩ total	5, 10, 20, 30, 40, 60, 80	9,6, 3.5, 3.5, 3, 3	HIMAC (SB3)
Ne (600)	Li, C, CH_2, Al, Cu, Pb, marsbar	ddx n/dΩ total	5, 10, 20, 30, 40, 60, 80	6, 5.5, 4, 3, 3, 3	HIMAC (PH2 and SB3)
Ar (95)	C, Al, Cu, Pb	ddx n/dΩ total	0, 30, 50, 80, 110	10 (all angles)	RIKEN
Ar (400)	C, Cu, Pb	ddx n/dΩ total	5, 10, 20, 30, 40, 60, 80	10, 7, 3.5, 3.5, 3, 3	HIMAC (PH2 and SB3)
Ar (560)	C, Cu, Pb, marsbar	ddx n/dΩ total	5, 10, 20, 30, 40, 60, 80	10, 7, 3.5, 3.5, 3, 3	HIMAC (PH2)
Fe (500)	Li, CH_2, Al	ddx n/dΩ total	5, 10, 20, 30, 40, 60, 80	12, 11, 7, 4, 3, 3	HIMAC (PH2)
Kr (400)	Li, C, CH_2, Al, Cu, Pb	ddx n/dΩ total	5, 10, 20, 30, 40, 60, 80	20 (all angles)	HIMAC (PH2)
Xe (400)	C, CH_2, Al, Cu, Pb	ddx n/dΩ total	5, 10, 20, 30, 40, 60, 80	10, 6, 5, 3.5, 3.5, 3.5	HIMAC (PH2 and SB3)

The range of projectile masses covers much of the range of GCR ions. Given that over half of the GCR flux is above 1 GeV/nucleon, however, there is a lack of data at those energies. He comprises approximately 8-9% of the GCR flux, and there is no data above 250 MeV/nucleon. Most of the existing measurements were taken at forward angles (≤ 90°), and all measurements had energy thresholds no lower than 3 MeV. Neutrons created at angles greater than 90° and at energies lower than 3 MeV are significant contributors to the neutron albedo created by GCR interactions in planetary atmospheres and surfaces, and as such indicates a need for data at those angles and energies.

In addition to secondary neutron production cross section measurements, there have been a number of "thick-target" measurements, where the targets are thick enough that there is appreciable neutron production via interactions of secondary particles created by primary beam interactions, as well as appreciable interactions of the neutrons as they transport through the target. In most cases, the targets are thick enough to stop the primary beam. These data are typically used as benchmarks for comparisons with transport model calculations, providing an overall test of the codes' abilities to handle primary and secondary interactions. Table II provides a compilation of secondary neutron yields from thick-target measurements[17].

Table II. Thick target measurements of secondary neutrons produced from the indicated beams and targets. Double differential (TTY), angular and energy differential, and total yields were measured as indicated. Spectra were measured at the given angles and energy thresholds. (From Ref. 17)

Beam ion and energy (MeV/nucleon)	Targets (cm)	Measured spectra	θ (deg)	Emin (MeV)
He (100)	C (5.0) Al (4.0) Cu (1.5) Pb (1.5)	TTY n/dΩ total	0, 7.5, 15, 30, 60, 90	5.5, 5, 4, 3.5, 3.5, 3
He (155)	Al (8.26)	TTY n/dΩ total	10, 30, 45, 60, 90, 125, 160	10, 3, 3, 7, 4, 3, 3
He (160)	Pb (3.937)	TTY Total	0, 45, 90, 120, 150	10, 3, 13, 13, 13
He (177.5)	C (14.73) H_2O (22.86) Steel (4.445) Pb (3.937)	TTY Total	0, 6, 15, 30, 45, 60, 90, 120, 135, 150	3, 10, 11, 11, 3, 10, 3, 13, 3, 13
He (180)	C (16.0) Al (12.0) Cu (4.5) Pb (5.0)	TTY n/dΩ total	0, 7.5, 15, 30, 60, 90	17, 11, 5.5, 6.5, 3.5, 3.5
C (100)	C (2.0) Al (1.0) Cu (0.5) Pb (0.5)	TTY n/dΩ total	0, 7.5, 15, 30, 60, 90	4, 4, 3.5, 3.5, 3, 3
C (155)	Al (8.26)	TTY n/dΩ total	10, 30, 45, 60, 90, 125, 160	10, 3, 3, 7, 4, 3, 3
C (180)	C (6.0) Al (4.0) Cu (1.5) Pb (1.5)	TTY n/dΩ total	0, 7.5, 15, 30, 60, 90	5.5, 5.5, 3.5, 2.5, 3, 2.5
C (400)	C (20.0) Al (15.0) Cu (5.0) Pb (5.0)	TTY n/dΩ total	0, 7.5, 15, 30, 60, 90	8.5, 5, 3.5, 3, 3, 3
Ne (100)	C (1.0)	TTY	0, 7.5, 15, 30, 60, 90	6, 6, 5, 5.5, 5.5, 5

	Al (1.0) Cu (0.5) Pb (0.5)	n/dΩ total		
Ne (180)	C (4.0) Al (3.0) Cu (1.0) Pb (1.0)	TTY n/dΩ total	0, 7.5, 15, 30, 60, 90	9,6, 3.5, 3.5, 3, 3
Ne (400)	C (11.0) Al (9.0) Cu (3.0) Pb (3.0)	TTY n/dΩ total	0, 7.5, 15, 30, 60, 90	6, 5.5, 4, 3, 3, 3
Si (800)	C (23.0) Cu (6.5)	TTY n/dΩ total	0, 7.5, 15, 30, 60, 90	11, 8, 8, 4, 3.5, 3.5
Ar (400)	C (7.0) Al (5.5) Cu (2.0) Pb (2.0)	TTY n/dΩ total	0, 7.5, 15, 30, 60, 90	10, 7, 3.5, 3.5, 3, 3
Fe (400)	C (6.0) Al (4.0) Cu (1.5) Pb (1.5)	TTY n/dΩ total	0, 7.5, 15, 30, 60, 90	12, 11, 7, 4, 3, 3
Nb (272)	Nb (1.0) Al (1.27)	TTY n/dΩ n/dE total	3, 6, 9, 12, 16, 20, 24, 28, 32, 36, 40, 48, 56, 64, 72, 80	20 (all angles)
Nb (435)	Nb (0.51)	TTY n/dΩ n/dE total	3, 6, 9, 12, 16, 20, 24, 28, 32, 36, 40, 48, 56, 64, 72, 80	20 (all angles)
Xe (400)	C (3.0) Al (2.0) Cu (1.0) Pb (1.0)	TTY n/dΩ total	0, 7.5, 15, 30, 60, 90	10, 6, 5, 3.5, 3.5, 3.5

All targets were composed of their natural ratio of isotopes. In contrast to the cross section measurements, some of the thick target experiments included measurements beyond 90 degrees in the lab. The beam energies ranged between 100 and 800 MeV/nucleon, and the minimum neutron energies were between 3 and 20 MeV.

Notably lacking in both the cross-section and thick-target measurements are experiments conducted for He projectiles above 200 MeV. He ions are the second-most abundant species in the GCR spectrum, and model predictions indicate that He interactions account for 25% - 30% of the neutron yield behind Al and polyethylene shielding.

V. Conclusion

Previous studies by the author and others have indicated that the main source of uncertainty in GCR transport model calculations of the radiation environment in enclosed, shielded spaces comes from the production of secondary light ions (p, d, t, ^{3}He, ^{4}He and neutrons). In order to reduce uncertainties in those calculations, the following are recommended for measurements at accelerator facilities:

1. Measurements of charged light ion secondaries and neutrons for He projectiles above 250 MeV/nucleon on targets of C, Al, Si, Fe, polyethylene, and other composities being developed for use in space
2. Measurements of charged secondary light ions from Fe projectiles above 100 MeV/nucleon on C, Al, Si, Fe targets
3. Measurements of charged secondary light ions from Si projectiles above 100 MeV/nucleon on C, Al, Si, Fe targets.

4. Measurements of HZE projectiles above 3 GeV/nucleon on targets of C, Al, Si and Fe. Preferred projectile species are H, He, C, O, Si, Ar, and Fe.
5. Thick-target measurements of secondary charged light ions that complement the existing double-differential cross section data.
6. Additional thick-target measurements of neutron yields from He projectiles above 250 MeV/nucleon.

References

[1]National Council on Radiation Protection and Measurements. Report No. 98 - Guidance on Radiation Received in Space Activities. NCRP report. NCRP, Bethesda, MD (1989). ISBN 9780929600048.

[2]National Council on Radiation Protection and Measure- ments. Report No. 132 - Radiation Protection Guidance for Activities in Low-Earth Orbit . NCRP report. NCRP, Bethesda, MD (2000). ISBN 0-929600-65-7.

[3]National Council on Radiation Protection et al.. Report No. 153 - Information Needed to Make Radiation Protec- tion Space Missions Beyond Low-Earth Orbit, NCRP report. NCRP, Bethesda, MD (2006). ISBN-13: 978-0-929600-90-1

[4]T. C. Slaba et al. Optimal shielding thickness for galactic cosmic ray environments. Life Sciences in Space Research 12, 1–15 (2017)

[5]T. Sato, et al., Features of Particle and Heavy Ion Transport code System (PHITS) version 3.02, J. Nucl. Sci. Technol. 55, 684-690 (2018).

[6]T. Goorley et al, "Initial MCNP6 Release Overview MCNP6 Version 1.0", (2013) LA-UR 13-22934

[7]T. Goorley, MCNP6.1.1-Beta Release Notes (2014) LA-UR-14-24680

[8]S. Agostinelli, et al. Geant4–a simulation toolkit, Nucl. Instr. Meth. Phys. A, 506 (2003), pp. 250-303

[9]A. Ferrari, et al., FLUKA: A Multi-Particle Transport Code (2005) CERN 2005-10 / SLAC-R-773.

[10] J. W. Wilson et al., Advances in NASA radiation transport research: 3DHZETRN Life Sci. Space Res., 2 (2014), pp. 6-22

[11] J. W. Wilson et al., 3DHZETRN: shielded ICRU spherical phantom, Life Sci. Space Res., 4 (2015), pp. 46-61

[12]J. W. Norbury , et al. Nuclear data for space radiation.Radiat Meas. (2012). 47:315–63. doi:10.1016/j.radmeas.2012.03.004

[13]J. W. Norbury, et al., Review of nuclear physics experiments for space radiation. NASA Technical Paper, NASA/TP-2011-217179, National Aeronautics and Space Administration, Washington DC (2011).

[14]J. W. Norbury, Nuclear physics and space radiation. J Phys Conf Ser. (2012). 381:012117. doi:10.1088/1742-6596/381/1/012117.

[15]J.W. Norbury et al., Review of nuclear physics experimental data for space radiation, Health Phys. (2012). 103:640–2. doi:10.1097/hp.0b013e318261fb7f

[16]J. W. Norbury et al., Are Further Cross Section Measurements Necessary for Space Radiation Protection or Ion Therapy Applications? Helium Projectiles, Front. Phys., 30 November 2020 Sec. Medical Physics and Imaging Volume 8 - 2020 | https://doi.org/10.3389/fphy.2020.565954

[17]T. Nakamura, L. Heilbronn, Handbook on Secondary Particle Production and Transport by High-energy Heavy Ions:(with CD-ROM), World Scientific, 2006.